Bonding of Graphite to Cu with Metal Multi-foils

Yuqi Cai[a], Biao Xu[a], Xinjian Ma[a], Julfikar Haider[b], Yangwu Mao[a,c,*], Shenggao Wang[a,*]

[a] Hubei Key Laboratory of Plasma Chemistry and Advanced Materials, Wuhan Institute of Technology, Wuhan 430205, China

[b] Department of Engineering, Manchester Metropolitan University, Manchester M1 5GD, UK

[c] Key Laboratory of Green Chemical Engineering Process of Ministry of Education, Wuhan Institute of Technology, Wuhan 430205, China

* Corresponding author, Email: myw@wit.edu.cn; wyysg@163.com

Tel: +86-27-87195661

Fax: +86-27-87195661

Abstract

Graphite/Cu bonding is essential for the fabrication of graphite-based plasma-facing parts and graphite-type commutators. Transient liquid phase bonding of graphite/Cu has been conducted separately with Ti/Cu/Ti and Ti/Cu/Ni/Ti multi-foils. The interfacial microstructure and mechanical properties of the bonded joints have been characterized. For the joint with Ti/Cu/Ti multi-foils, complete melting of the Ti/Cu/Ti multi-foils and interdiffusion between the molten zone and the Cu substrate occur during the bonding process, leading to formation of Ti-Cu intermetallics in the bonding area. The liquid phase flowing towards sidewall of the Cu substrate gives rise to a thickness of the bonding area far less than those of the as-received multi-foils. For the joint with Ti/Cu/Ni/Ti multi-foils, the bonding area can be divided into three parts (areas I, II and III). The bonding areas I and III are comprised of Ti-Cu intermetallics and $Ti(Cu_xNi_{1-x})_2$, while the bonding area II consists of a Ni layer and two thin $TiNi_3$ reaction layers. The thickness of the whole bonding area is similar to those of the as-received multi-foils, indicating that addition of Ni foil can prevent the loss of liquid phase zone by inhibiting the excessive liquid phase formation. The addition of a Ni foil in bonding of the graphite/Cu may alleviate the joint residual stress by its intermediate coefficient of thermal expansion (CTE) to accommodate any thermal mismatch in the joint and by its superior ductility and plasticity, thus resulting in shear strength promotion of the joint with the Ti/Cu/Ni/Ti multi-foils by approximately 35% when compared to the Ti/Cu/Ti multi-foils.

Keywords

Bonding · Brazing · Metal foil · Microstructure · Mechanical properties

1 Introduction

Graphite/Cu bonding is essential for the fabrication of graphite-based plasma-facing parts in nuclear fusion reactor and graphite-type commutator in automobile industry [1]. However, the main challenges involved in graphite/Cu bonding include poor wetting of Cu on graphite and joint residual stress generated by their large thermal mismatch upon bonding at high temperature [2]. In order to promote the wetting behavior between graphite and Cu, brazes containing active metal such as Ti and Cr have been employed in graphite/Cu joining. Li et al. [3] brazed graphite to Cu with Ag-27.5Cu-1.0Al-2.5Ti filler at 850 ºC and obtained a joint with shear strength of 15 MPa. Zhang et al. [4] studied graphite/Cu brazing with Ni-12.6Cr-9P-10Cu at 950 ºC and detected a chromium carbide reaction layer close to the graphite side. In our previous study, graphite/Cu brazing was also achieved with Cu-TiH_2 based fillers [5,6].

Furthermore, transient liquid phase bonding (TLPB), based on formation of liquid phase by the eutectic reaction between metal foils or between metal foil and metal substrate, is an alternative technique for joining dissimilar materials [7]. Ti metal foil has been used to create a good bond between graphite and Cu by TLPB due to the formation of a eutectic phase between the Ti foil and Cu substrate [8].

The joint residual stress in dissimilar materials joining may be detrimental for the joint mechanical properties and reliability in practical applications. A metal foil with good plasticity and intermediate coefficient of thermal expansion (CTE) is frequently introduced to accommodate the thermal mismatch in the joint or to transfer the stress concentration in the dissimilar materials joining, consequently leading to the relief of joint residual stress [9-12]. Hao et al. [11] applied a Cu foil in C/C composite/Ti_2AlNb alloy brazing to relax the joint residual stress. Xing et al. [12] introduced a Nb foil to reduce the joint residual stress in the bonding of graphite/Cu.

The fillers applied in graphite/Cu brazing show some disadvantages such as high cost (Ag-Cu-Al-Ti filler [3]), unsatisfactory conductivity of the brazing area (Ni-Cr-P-Cu filler [4]) and complicated preparation processing (Cu-TiH_2+C composite filler [5]). In contrast, the bonding of graphite to Cu with Ti/Cu/Ti multi-foils is promising due to its low cost and convenient application processing. In addition, taking into account the existence of residual stress in graphite/Cu bonding, an addition of a Ni foil in Ti/Cu/Ti multi-foils may contribute to relief of the joint residual stress due to its superior plasticity and intermediate CTE between those of graphite and Cu. Hence, in this study bonding of graphite/Cu was conducted separately with Ti/Cu/Ti and Ti/Cu/Ni/Ti multi-foils in vacuum atmosphere. The joint microstructure and mechanical properties were extensively studied, and the effect of Ni foil on relieving the joint residual stress was discussed.

2 Experimental Procedures

Graphite with an average density of 1.9 g cm^{-3} and Cu with an average density of 8.9 g cm^{-3} were used as the bonding substrates. The graphite and Cu substrates with same dimensions of 10 × 10 × 10 mm^3 were acquired from Beijing Jinglong Special Carbon Company, China and Beijing Tiancheng Jida Metal Company, China, respectively. The Cu, Ti and Ni foils with purities of 99.9%, 99.6% and 99.9% and nominal thicknesses of 50 μm, 30 μm and 50 μm, respectively, were obtained from Qinghe Guantai Metal Company, China. The bonding surfaces of graphite, Cu and metal foils were polished with a 1000-grit SiC sandpaper to remove any surface contaminants, and then immersed in ethanol to conduct ultrasonic cleaning for 30 min.

Bonding of graphite/Cu was carried out in a high-temperature furnace under vacuum better than 5 × 10^{-3} Pa. Fig. 1 shows schematic diagram of the bonding assemblies. The graphite/Cu bonding with the Ti/Cu/Ti and Ti/Cu/Ni/Ti multi-foils was assembled in the orders of graphite/Ti foil/Cu foil/Ti foil/Cu substrate and graphite/Ti foil/Cu foil/Ni foil/Ti foil/Cu substrate, respectively. In order to promote the bonding among the metal multi-foils and substrates, the bonding assemblies were subjected to a load of approximately 9.6 kPa. The bonding temperature in this study was set at 950 °C to ensure melting of the metal multi-foils. The assemblies were first heated to 800 °C at a heating rate of 10 °C min^{-1} from room temperature (25 °C), and then to 950 °C at a rate of 5 °C min^{-1}. After holding at 950 °C for 30 min, the bonding assemblies were cooled to approximately 25 °C by furnace cooling.

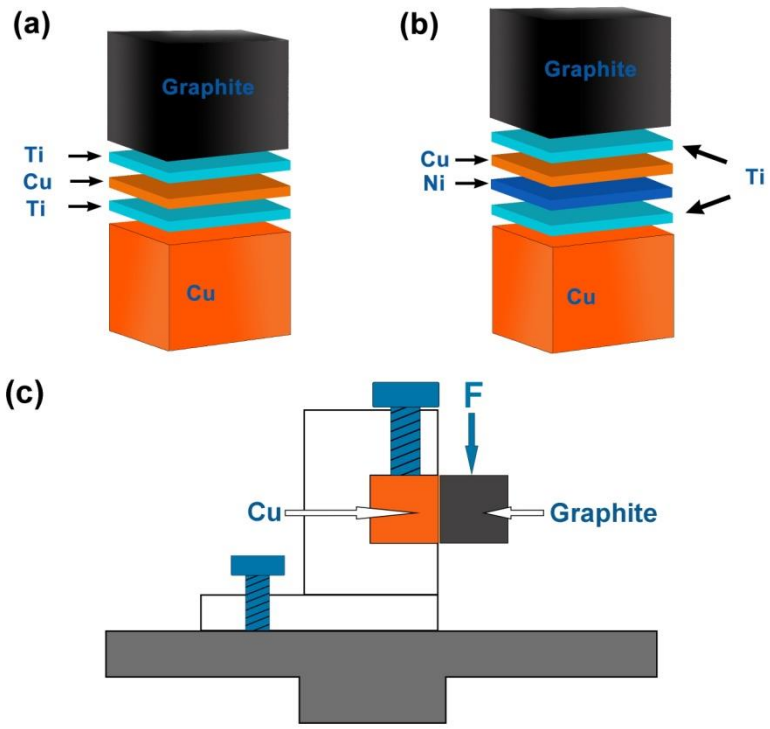

Fig. 1 Schematics of assemblies for graphite/Cu bonding with **a** Ti/Cu/Ti multi-foils and **b** Ti/Cu/Ni/Ti multi-foils as well as **c** schematic diagram of shear test for graphite/Cu joints

The microstructure and corresponding elemental compositions of the bonding area in the graphite/Cu joint were characterized by a field emission scanning electron microscope (FESEM, GeminiSEM 300) equipped with an energy-dispersive X-ray spectrometer (EDS, Oxford Inca X-Act). The FESEM images were captured in backscattered electron (BSE) mode. The phase identification in the bonding area of the joints was performed by an X-ray diffraction spectrometer (XRD, Bruker D8 Advance) using Cu-Kα radiation with a wavelength of 0.15418 nm and a scanning speed of 4° min^{-1}.

The microhardness distributions and apparent shear strengths in the graphite/Cu joints were determined by following the measurement procedures illustrated by Duan et al. [13]. The microhardness values in the bonding area and the Cu substrate in the joints were measured to further verify the phase formation in the graphite/Cu joint. The shear tests of graphite/Cu joints, as schematically shown in Fig. 1c), were conducted by an electronic universal materials testing machine (GP-TS2000s) at room temperature with a displacement rate of 0.5 mm/min. The shear strength was calculated by dividing the maximum load by the joining area of the joint. Five samples bonded with same bonding condition were measured to obtain the average joint shear strength. The 3D depth fracture-surface images of the joints after shear tests were captured by a Digital Microscope (Keyence VHX-7000).

3 Results and Discussion

3.1 Microstructure of Joint with Ti/Cu/Ti Multi-foils

The morphology and EDS mappings of the graphite/Cu joint with Ti/Cu/Ti multi-foils are shown in Fig. 2. The bonding area consisting of light-gray region and dark-gray particle-like region is found to be defect-free, indicating a desirable interfacial bonding of the metal foils with the graphite and Cu substrates. The EDS mappings in Fig. 2b-d) show that the bonding area contains Ti and Cu elements, implying the inter-diffusions among the Ti/Cu/Ti multi-foils and the Cu substrate. Notably, the wave-like interfacial structure between the bonding area and Cu substrate suggest the dissolution of Cu substrate into the liquid phase zone during the bonding.

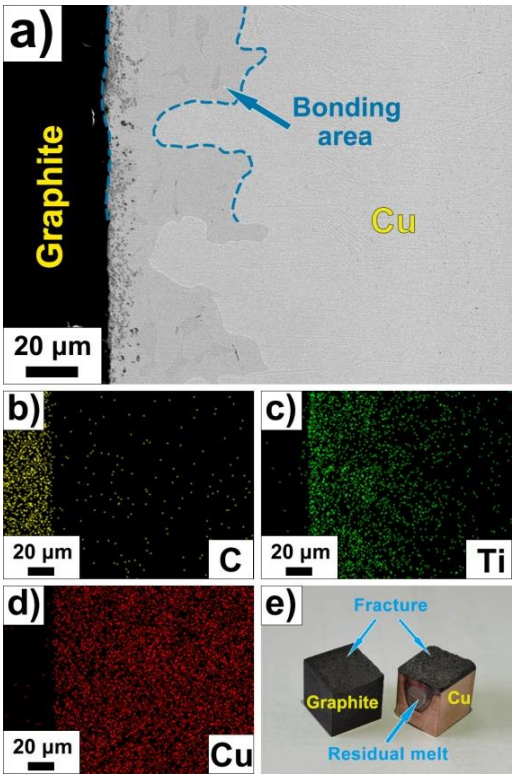

Fig. 2 a Morphology, **b-d** EDS mappings and **e** fracture images after shear testing of the graphite/Cu joint with Ti/Cu/Ti multi-foils

Furthermore, the thickness of the bonding area varied from around 20 μm to 60 μm, significantly less than those of the as-received multi-foils (110 μm). This indicates significant loss of the molten zone in the bonding area during the bonding. For graphite/Cu bonding with the Ti/Cu/Ti multi-foils, the liquid phase zones occur at three interfaces (Ti foil/Cu foil, Cu foil/Ti foil and Ti foil/Cu substrate interfaces) when the bonding temperature is higher than the Ti-Cu eutectic temperature (875 °C). The relatively high bonding temperature and long dwelling time (30 min) may lead to rapid melting of the Ti/Cu/Ti multi-foils. Hence, some liquid phase may flow away along the sidewall of the Cu substrate under action of the applied shear load (see the residual melt on the sidewall of Cu substrate in Fig. 2e), resulting in thickness reduction of the bonding area.

Fig. 3 displays FESEM image and EDS mappings of the magnified graphite/bonding area in the joint with the Ti/Cu/Ti multi-foils. The bonding area consists of a uniform light-gray region and a particle-like region. The EDS mapping of Ti in Fig. 3b) reveals that Ti element enriches at the graphite/bonding area interface, suggesting the formation of a thin TiC reaction layer.

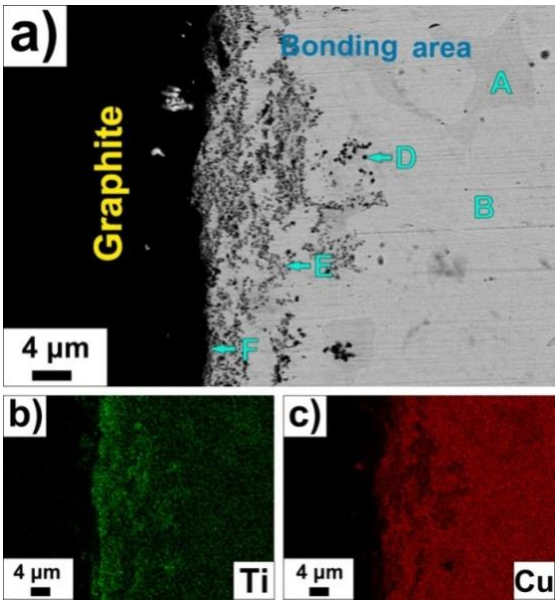

Fig. 3 a FESEM image and **b-c** EDS mappings of the magnified graphite/bonding area in the graphite/Cu joint with Ti/Cu/Ti multi-foils

The elemental compositions and deduced phases of the micro-regions marked in Fig. 3a) are shown in Table 1. The gray micro-region A containing 34.56 at.% Ti and 65.44 at.% Cu is inferred as $TiCu_2$. The detection of $TiCu_2$ in the bonding area was also reported by Ehsan et al. [14] in Ti6Al4V/AISI 304 steel bonding with Cu interlayer and by Elrefaey and Tillmann [15] in Ti/low carbon steel bonding with Cu-12Mn-2Ni (wt %) interlayer. For the light-gray micro-region B, the atomic ratio of Ti/Cu is about 1:4, corresponding to $TiCu_4$. Lin et al. [8] also detected $TiCu_4$ phase in the bonding area for the graphite/Cu joint bonded with Ti foil at 920 °C. Similarly, the dark-gray micro-region D and gray micro-region E in the particle-like region provide Ti/Cu atomic ratio of 2:1 and 1:1 respectively, determined as Ti_2Cu and TiCu, respectively. The micro-region F adjacent to the graphite substrate consists of 12.84 at.% C, 69.56 at.% Ti and 17.60 at.% Cu, deduced as a mixture of TiC and Ti-Cu. The formation of thin TiC reaction layer at the graphite/Ti-containing filler interface has been confirmed by Vidyuk et al. [16] in graphite/Cu bonding with Ti-Cu filler and by Wei et al. [17] in graphite/Cu brazing with Cu-50TiH_2 filler.

Table 1 Elemental compositions and deduced phases of the marked micro-regions in Fig. 3a)

Micro-regions	Compositions (at.%)			Deduced phases
	C	Ti	Cu	

A	-	34.56	65.44	$TiCu_2$
B	-	21.76	78.24	$TiCu_4$
D	-	65.21	34.79	Ti_2Cu
E	-	54.24	45.76	TiCu
F	12.84	69.56	17.60	TiC, Ti-Cu

Fig. 4 shows XRD pattern of the bonding area in the graphite/Cu joint with Ti/Cu/Ti multi-foils. The XRD result indicates that the measured area contains TiCu, $TiCu_4$, Ti_2Cu, $TiCu_2$, TiC, C and Cu phases. The identification of intermetallics in the XRD result is consistent with the EDS results, confirming that the bonding area is composed of Ti-Cu intermetallics. The detection of TiC suggests the development of TiC reaction layer close to the graphite side. The C and Cu peaks in the XRD result may originate from the graphite and Cu substrates, respectively.

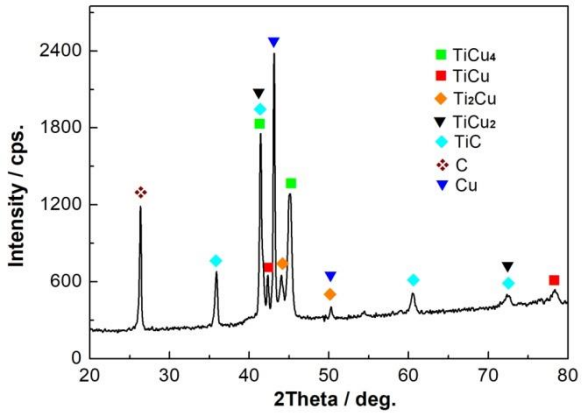

Fig. 4 XRD result of the bonding area in the graphite/Cu joint with Ti/Cu/Ti multi-foils

Fig. 5 depicts interface evolution involved in graphite/Cu bonding with Ti/Cu/Ti multi-foils. The interface can be roughly divided into four stages: initial liquid phase formation, partial liquid phase, complete liquid phase and cooling.

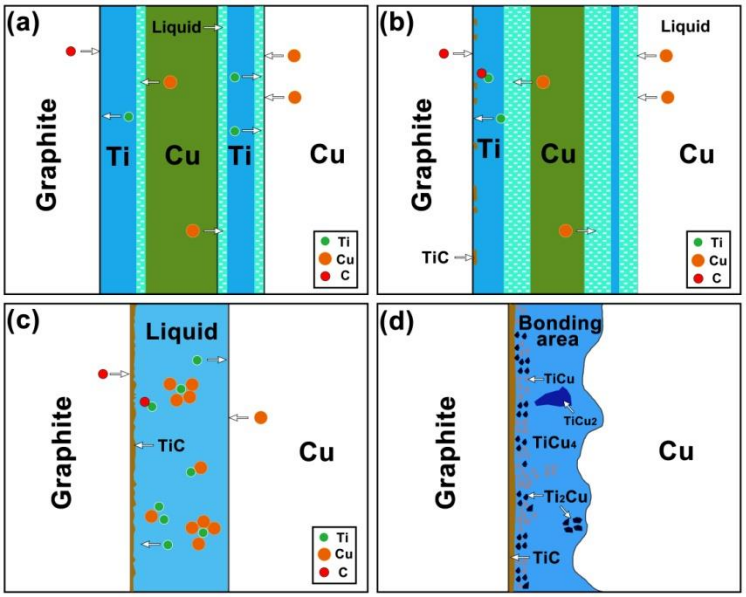

Fig. 5 Schematic diagrams of interface development for bonding of graphite/Cu with Ti/Cu/Ti multi-foils: **a** Initial liquid phase formation stage; **b** Partial liquid phase stage; **c** Complete liquid phase stage and **d** Cooling stage

In the first stage (Fig. 5a), thin liquid phase layers are developed at three interfaces (including Ti foil/Cu foil, Cu foil/Ti foil and Ti foil/Cu substrate) when the temperature exceeds the eutectic temperature of Ti-Cu alloy. Meanwhile, inter-diffusion of carbon and Ti atoms occurs at the graphite/Ti foil interface due to a high chemical affinity of the active metal Ti with graphite, leading to the formation of TiC particles. With an increase of the bonding temperature, rapid dissolution of the solid metal foils into the liquid phase zones may accelerate melting of the metal multi-foils, resulting in an increase of the liquid phase zones as shown in Fig. 5b).

When the metal multi-foils completely melt (Fig. 5c), some liquid phase may infiltrate into the open pores of the graphite substrate and some may flow along the sidewall of the Cu substrate under the action of applied load, leading to a reduction in thickness of the bonding area. At the same time, partial dissolution of Cu into the liquid phase zone takes place. Furthermore, a continuous TiC reaction layer is formed at the graphite/liquid phase interface. During the cooling stage (Fig. 5d), the grains of Ti-Cu intermetallics including $TiCu_4$, TiCu, $TiCu_2$ and Ti_2Cu start to precipitate from the liquid phase zone, leading to the formation of Ti-Cu intermetallics in the bonding area of the joint.

3.2 Microstructure of Joint with Ti/Cu/Ni/Ti Multi-foils

Fig. 6 displays FESEM morphology and EDS mappings of the graphite/Cu joint with the Ti/Cu/Ni/Ti multi-foils. The FESEM image in Fig. 6a) reveals satisfactory interfacial bonding among the metal multi-foils and the substrates. The bonding area can be divided into three parts, namely areas I, II and III. The areas I and III are both composed of light-gray region and gray region, whereas the bonding area II contains uniform gray region.

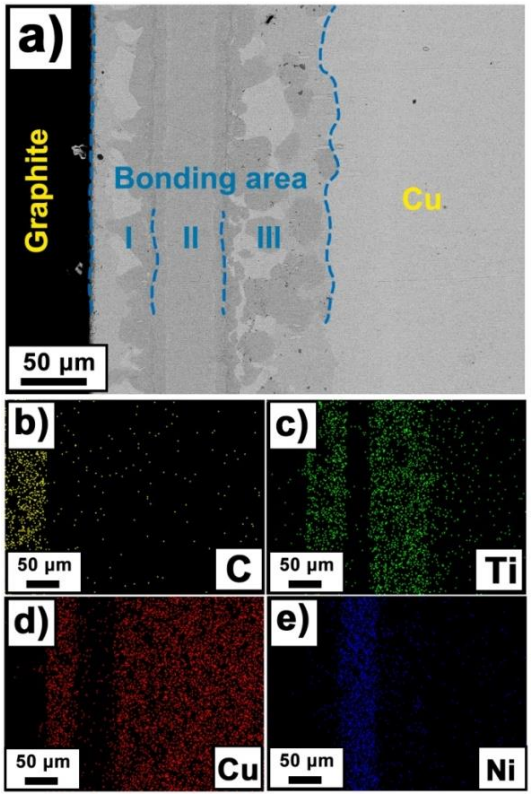

Fig. 6 a Morphology and **b-e** EDS mappings of the graphite/Cu joint with Ti/Cu/Ni/Ti multi-foils

The EDS mappings shown in Fig. 6b-e) reveal that both the bonding areas I and III are Ti- and Cu-rich, confirming the melting of Ti and Cu foils during the bonding. The bonding area II is Ni-rich, implying limited dissolution of the Ni foil into the Ti-Cu liquid phase zones. Based on the Cu-Ni alloy phase diagram [18], the liquidus temperature of Cu-Ni alloy is higher than the melting point of Cu (1084 ºC). Thus, it is almost unlikely to create a liquid phase at the Cu foil/Ni foil interface at the bonding temperature of 950 ºC. Also, significant dissolution of Ni foil into the liquid phase zones is negligible since the Ti-Ni eutectic temperature (942 ºC [18]) is highly close to the bonding temperature.

It should be noted that the whole bonding area in the joint exhibits a thickness of approximately 170 μm, which is close to the combined thickness of the as-received Ti/Cu/Ni/Ti multi-foils (160 μm). This implies that addition

of the Ni foil in the bonding of graphite/Cu can prevent the liquid phase flowing towards the sidewall of Cu substrate.

Fig. 7 shows magnified FESEM images of the interfacial area in the graphite/Cu joint with the Ti/Cu/Ni/Ti multi-foils. Two thin layers (marked as R1 and R2 in Fig. 7b) with similar thickness of about 5 μm can be distinguished in the bonding area II. Table 2 gives elemental compositions of the micro-regions in Fig. 7.

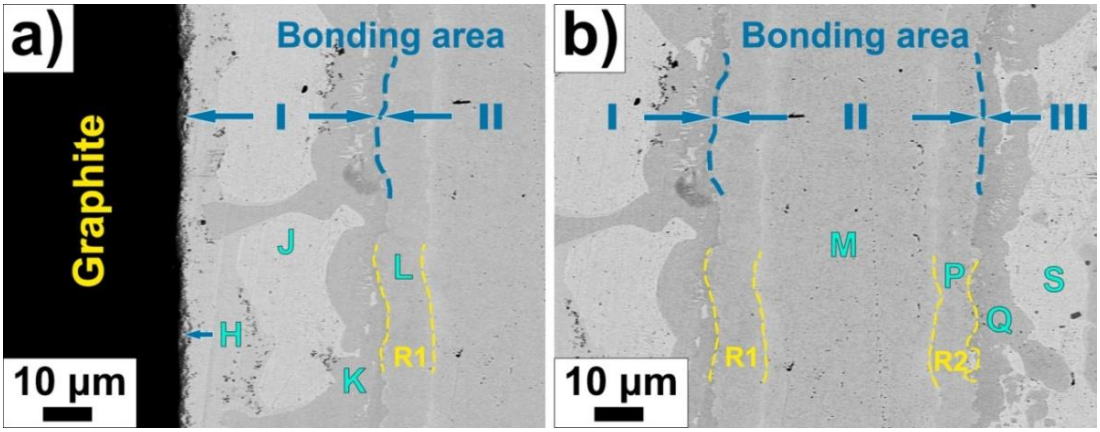

Fig. 7 Magnified FESEM images of the interfacial area in the graphite/Cu joint with Ti/Cu/Ni/Ti multi-foils: **a** Graphite/bonding area and **b** Bonding area

Table 2 Elemental compositions and deduced phases of the marked micro-regions in Fig. 7

Micro-regions	Compositions (at.%)				Deduced phases
	C	Ti	Cu	Ni	
H	13.21	55.79	31.00	-	TiC, Ti-Cu
K	-	32.95	54.44	12.61	$Ti(Cu_xNi_{1-x})_2$
J	-	27.92	72.08	-	$TiCu_4$
L	-	28.61	-	71.39	$TiNi_3$
M	-	-	-	100.00	Ni
P	-	27.38	-	72.62	$TiNi_3$
Q	-	32.89	52.20	14.91	$Ti(Cu_xNi_{1-x})_2$
S	-	10.79	89.21	-	$TiCu_4$

The micro-region H at the graphite/bonding area interface contains Ti, Cu and C, suggesting the formation of TiC and Ti-Cu. For both the gray micro-regions K in the bonding area I and Q in the area III, the atomic ratios of Ti/Cu+Ni are around 1:2, and determined as $Ti(Cu_xNi_{1-x})_2$. Mao et al. [19] also detected $Ti(Cu_xNi_{1-x})_2$ phase in graphite/CuCrZr alloy brazing with Cu-TiH_2-Ni filler. The light-gray micro-regions J in the bonding area I and S in the area III are both inferred as $TiCu_4$ based on the Ti/Cu atomic ratios.

The micro-region M in the bonding area II contains 100 at.% Ni, suggesting that Ni foil undergoes limited interaction with the liquid phase zones. For the gray micro-regions L in the R1 layer and P in the R2 layer, the atomic ratios of Ti to Ni are both close to 1:3, suggesting the formation of two $TiNi_3$ reaction layers on both sides of the Ni foil. Buenconsejo et al. [20] claimed that $TiNi_3$ phase was formed in the Ti-Ni-W composites due to the reaction of Ti with Ni. Furthermore, Watanabe et al. [21] reported that Ti was inclined to react with Ni to form Ti-Ni intermetallics other than with Cu since the mixing enthalpy of Ti-Ni (-40.17 kJ mol^{-1}) was lower than that of the Ti-Cu (-3.67 kJ mol^{-1}). Arroyave and Eagar [22] also demonstrated that the enthalpy of Ti-Ni interaction (-187 kJ mol^{-1}) was much lower than that of the Ti-Cu interaction (-10 kJ mol^{-1}). Therefore, in the Cu-Ni-Ti ternary system, Ti tends to react more with Ni to create Ti-Ni intermetallics instead of Cu to form Ti-Cu intermetallics.

Fig. 8 displays schematic of measured faces for XRD characterization and corresponding XRD patterns of the bonding area in the graphite/Cu joint with Ti/Cu/Ni/Ti multi-foils. As shown in Fig. 8a), the face A located at the graphite/bonding area interface and the face B close to the bonding area I/II interface have been characterized by XRD. The XRD result in Fig. 8b) shows that phases including $TiCu_4$, Ti_2Cu, TiCu, TiC, $Ti(Cu_xNi_{1-x})_2$, C and Cu exist in the face A. The detection of $TiCu_4$, Ti_2Cu, TiCu and $Ti(Cu_xNi_{1-x})_2$ is consistent with the EDS results, confirming that the bonding area I is comprised of Ti-Cu intermetallics and $Ti(Cu_xNi_{1-x})_2$. The identification of TiC indicates the formation of a TiC layer at the graphite/bonding area interface, similar to that obtained in the joint with the Ti/Cu/Ti multi-foils. Moreover, the detection of carbon and Cu may be attributed to the graphite and Cu substrates, respectively. The XRD pattern of the face B reveals the existences of $TiNi_3$ and Ni besides the phases including $TiCu_4$, Ti_2Cu, TiCu and $Ti(Cu_xNi_{1-x})_2$ and Cu, confirming the formation of $TiNi_3$ reaction layers on both sides of the Ni layer.

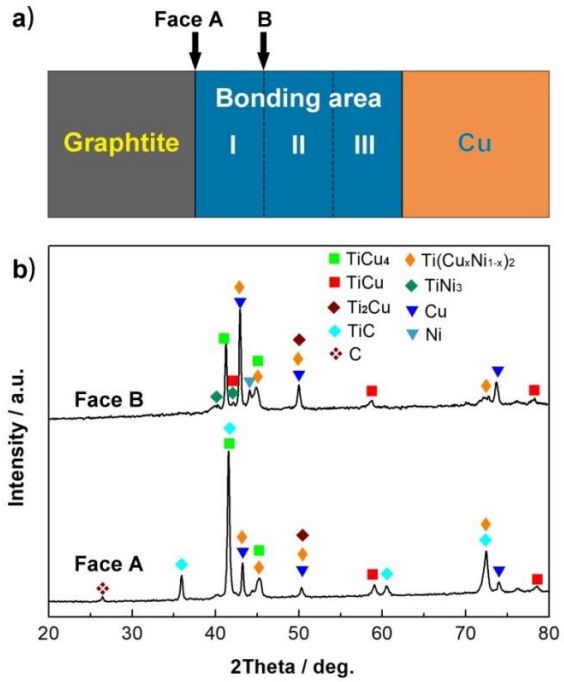

Fig. 8 a Schematic of measured faces for XRD characterization and **b** corresponding XRD patterns of the bonding area in the graphite/Cu joint with Ti/Cu/Ni/Ti multi-foils

3.3 Mechanical Characterizations

Fig. 9 shows microhardness distributions of the graphite/Cu joints with Ti/Cu/Ti and Ti/Cu/Ni/Ti multi-foils. The microhardness of the bonding area in the joint with Ti/Cu/Ti multi-foils is 360 ± 14 $HV_{0.1}$, in agreement with that reported by Konieczny [23], who claimed that the microhardness values of Ti-Cu intermetallics such as $TiCu_4$ and Ti_2Cu were in the range of 273 to 681 HV. For the joint with Ti/Cu/Ni/Ti multi-foils, the bonding areas I and III exhibit microhardness values of 329 ± 55 $HV_{0.1}$ and 326 ± 27 $HV_{0.1}$, respectively, comparable to that with the Ti/Cu/Ti multi-foils due to similar phases formed in the bonding area. The bonding area II (mainly the Ni layer) in the joint with Ti/Cu/Ni/Ti multi-foils displays a microhardness of 164 ± 9 $HV_{0.1}$, similar to that obtained by Xiong et al. [24] in Al/Cu diffusion bonding with Ni foil (171 HV).

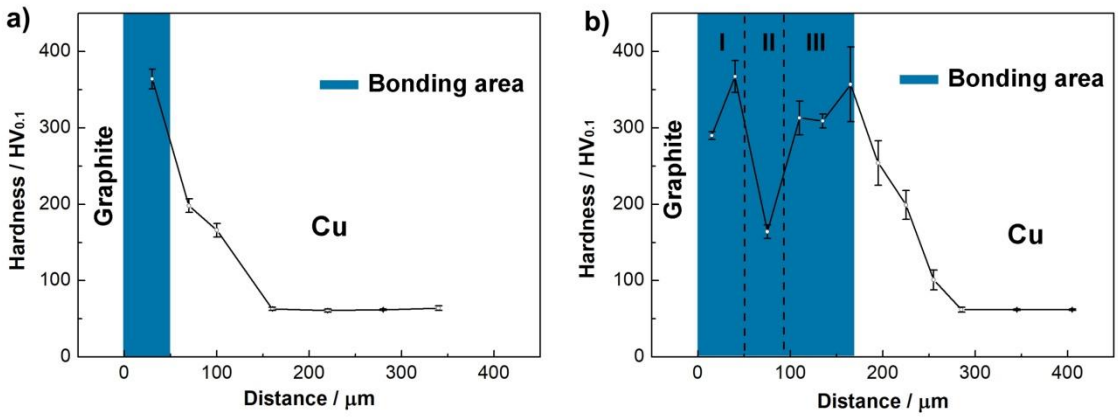

Fig. 9 Microhardness distributions of the graphite/Cu joints with **a** Ti/Cu/Ti multi-foils and **b** Ti/Cu/Ni/Ti multi-foils

Furthermore, the microhardness values of the Cu parts in the joints with Ti/Cu/Ti multi-foils and Ti/Cu/Ni/Ti multi-foils vary from 198 ± 9 $HV_{0.1}$ to 63 ± 3 $HV_{0.1}$ and from 254 ± 29 $HV_{0.1}$ to 62 ± 1 $HV_{0.1}$ respectively (at distances about 0 ~ 120 μm from the bonding area/Cu substrate interface). As revealed by the joint microstructure characterization, the diffusion of Ti into the Cu substrate in the area close to the bonding area/Cu substrate interface is more significant than that far away from the interface for both the joints. Thus, the Cu substrate near the interface exhibits a higher microhardness than that further away from the interface, since the microhardness of the solid solution is relatively higher than that of base metal [25]. The hardness of Cu substrate at a distance of approximately 120 μm away from the bonding area/Cu interface is in agreement with that measured by Dai et al. [26] (60 HV). Based on the microhardness results above, one can see that the microhardness distributions in the graphite/Cu joints with metal multi-foils are chiefly related to their phase formation.

Fig. 10 shows the shear strength and load-displacement curves of the graphite/Cu joints with the Ti/Cu/Ti and Ti/Cu/Ni/Ti multi-foils. The shear strength of the joint with Ti/Cu/Ti multi-foils is 12.9 ± 0.6 MPa (about 85 % of the graphite substrate strength, 15.2 ± 1.4 MPa), indicating a favorable interfacial bonding of graphite to Cu. For the joint with the Ti/Cu/Ni/Ti multi-foils, the shear strength increases to 17.5 ± 1.9 MPa, implying that the addition of Ni foil in Ti/Cu/Ti multi-foils contributes to the improvement in the joint strength. Moreover, it is noticeable that the shear strength of joint with Ti/Cu/Ni/Ti multi-foils is higher than that of graphite substrate, which is attributed to the strengthening of the graphite substrate by the liquid filler infiltration into the graphite open pores.

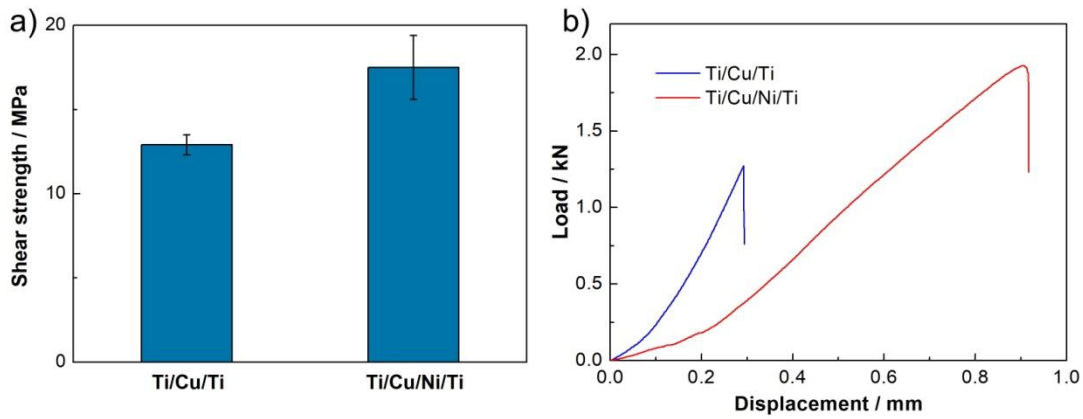

Fig. 10 a Shear strength and **b** load–displacement curves of the graphite/Cu joints with Ti/Cu/Ti and Ti/Cu/Ni/Ti multi-foils

As Kang et al. [9] claimed, introduction of a metal foil with intermediate CTE in dissimilar materials joining was beneficial for the relaxation of joint residual stress by accommodating thermal mismatch in the joint. Thus, application of the Ni foil in graphite/Cu bonding can effectively decrease the thermal mismatch within the joint since the CTE of Ni foil (13.4×10^{-6} $^{o}C^{-1}$ [27]) is in the range between those of graphite (4.8×10^{-6} $^{o}C^{-1}$ [28]) and Cu (16.7×10^{-6} $^{o}C^{-1}$ [28]). Zhong et al. [29] also applied Mo foil with a CTE of 5×10^{-6} $^{o}C^{-1}$ [30] to accommodate the CTE mismatch between graphite and Cu, therefore alleviating the joint stress.

Furthermore, the relaxation of joint residual stress can be achieved by the superior plasticity and ductility of the Ni foil. Ba et al. [31] claimed that introduction of Ni foil with good plasticity in C/C composite/Ni-based superalloy brazing could allow the shrinkage of the filler layer and result in the relaxation of joint stress. Chen et al. [32] attributed the partial dissipation of joint residual stress to the excellent plasticity of Ni foil in Zr–Sn–Nb alloy/304 stainless steel bonding. Niu et al. [33] also reported that the Ni foil with the thickness of 60~120 μm could significantly decrease the residual stress of Ti-Zr-Mo alloy/Ti_2AlNb joint.

The fracture and 3D depth fracture-surface images of the joints with Ti/Cu/Ti and Ti/Cu/Ni/Ti multi-foils are shown in Fig. 11. The fracture images reveal that fracture occurs in the graphite side close to the bonding area of both the joints. This kind of fracture is generally caused by the stress concentration in the graphite side or by the relatively low strength of graphite substrate. Taking into account that the shear strength of the joint with Ti/Cu/Ti multi-foils (12.9 ± 0.6 MPa) is lower than that of graphite substrate (15.2 ± 1.4 MPa), the fracture may be attributed to the residual stress in the graphite/Cu joint. The bowl-shape fracture in Fig. 11a-b) also suggests the existence of residual stress in the graphite/Cu joint with Ti/Cu/Ti multi-foils.

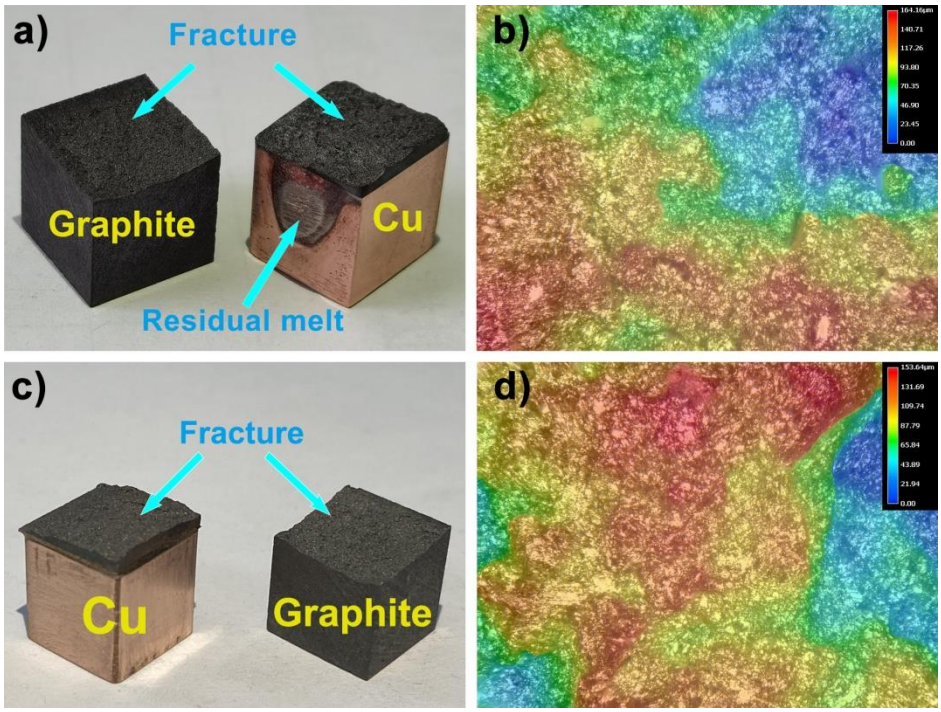

Fig. 11 Fracture and 3D depth fracture-surface images of the graphite/Cu joints with **a-b** Ti/Cu/Ti and **c-d** Ti/Cu/Ni/Ti multi-foils

For the joint with Ti/Cu/Ni/Ti multi-foils, the fracture images in Fig. 11c-d) show a rough fracture surface. Xing et al. [12] demonstrated that the rugged fracture implied the consumption of high fracture energy by the crack deflection, leading to a higher joint strength. Thus, the rough fracture-surface in the joint with Ti/Cu/Ni/Ti multi-foils suggests that the residual stress in the joint was partially relieved by the addition of Ni foil, consequently resulting in an improvement of the joint strength. Notably, the shear strength of joint with Ti/Cu/Ni/Ti multi-foils is higher than that of the graphite substrate, suggesting that the fracture is caused by the relatively low strength of the graphite substrate. Furthermore, no cracks are observed at the graphite/bonding area and bonding area/Cu interfaces, implying that favorable bonding is achieved among the graphite, multi-foils and Cu substrates.

4 Conclusions

1) Bonding of graphite/Cu has been achieved with Ti/Cu/Ti multi-foils and Ti/Cu/Ni/Ti multi-foils in vacuum atmosphere.

2) For the joint with Ti/Cu/Ti multi-foils, the bonding area is mainly composed of Ti-Cu intermetallics. A TiC reaction layer is formed at the graphite/bonding area interface. In addition, a large amount of liquid phase flowing

to the sidewall of Cu substrate gives rise to a thickness reduction in the bonding area.

3) For the joint with Ti/Cu/Ni/Ti multi-foils, the bonding area consists of three areas (I, II and III). The bonding areas I and III are comprised of Ti-Cu intermetallics and $Ti(Cu_xNi_{1-x})_2$, while the bonding area II consists of a Ni layer and two thin $TiNi_3$ reaction layers.

4) The joints with Ti/Cu/Ti multi-foils and Ti/Cu/Ni/Ti multi-foils exhibit the shear strengths of 12.9 ± 0.6 MPa and 17.5 ± 1.9 MPa, respectively. The addition of Ni foil in the bonding of graphite/Cu can alleviate the joint residual stress by its intermediate coefficient of thermal expansion (CTE) to accommodate the thermal mismatch in the joint and by its superior ductility and plasticity.

References

1. Diop S, Rigaud E, Cornuault PH, Grandais-Menant E, Bazin B. Experimental analysis of the vibroacoustic response of an electric window-lift gear motor generated by the contact between carbon brushes and commutators. J Vib Acoust Trans ASME. 2017;139(6):061002. https://doi.org/10.1115/1.4036869.
2. Zhang LX, Zhang B, Sun Z, Tian XY, Lei M, Feng JC. Preparation of the graphene nanosheets reinforced AgCuTi based composite for brazing graphite and Cu. J. Alloys Compd. 2019;782:981-985. https://doi.org/10.1016/j.jallcom.2018.11.407.
3. Li C, Si XQ, Cao J, Qi JL, Dong ZB, Feng JC. Residual stress distribution as a function of depth in graphite/copper brazing joints via X-ray diffraction. J. Mater. Sci. Technol. 2019;32:2470-2476. https://doi.org/10.1016/j.jmst.2019.07.023.
4. Zhang J, Wang TP, Liu CF, He YM. Effect of brazing temperature on microstructure and mechanical properties of graphite/copper joints. Mater Sci Eng A. 2014;594:26-31. https://doi.org/10.1016/j.msea.2013.11.059.
5. Mao YW, Wang S, Peng LX, Deng QR, Zhao P, Guo BB, Zhang YZ. Brazing of graphite to Cu with $Cu50TiH_2$+C composite filler. J Mater Sci. 2016;51(4):1671-1679. https://doi.org/10.1007/s10853-015-9415-0.
6. Mao YW, Yu S, Zhang YZ, Guo BB, Ma ZB, Deng QR. Microstructure analysis of graphite/Cu joints brazed with (Cu-$50TiH_2$)+ B composite filler. Fusion Eng Des. 2015;100:152-158. https://doi.org/10.1016/j.fusengdes.2015.05.011.
7. Jiang QY, Wang YJ, Xu HM, Ma XJ, Wang SG, Mao YW. Transient liquid phase bonding of graphite to

Ti6Al4V alloy. Sci Technol Weld Joining. 2022; 27(8): 615-620. https://doi.org/10.1080/13621718.2022.2095195

8. Lin JC, Huang M, Yang WQ, Xing LL. Degradation kinetics of Ti-Cu compound layer in transient liquid phase bonded graphite/copper joints. Sci Rep. 2018;8(1):1-11. https://doi.org/10.1038/s41598-018-33446-3.
9. Kang YH, Feng KM, Zhang WT, Mao YW. Microstructural and mechanical properties of CFC composite/Ti6Al4V joints brazed with Ag-Cu-Ti and refractory metal foils. Arch Civ Mech Eng. 2021;21(3):113. https://doi.org/10.1007/s43452-021-00268-6.
10. Gao YA, Huang LJ, Bao Y, An Q, Sun Y, Zhang R, Geng L, Zhang J. Joints of TiBw/Ti6Al4V composites-Inconel 718 alloys dissimilar joining using Nb and Cu interlayers. J Alloys Compd. 2020;822:153559. https://doi.org/10.1016/j.jallcom.2019.153559.
11. Hao ZT, Wang DP, Yang ZW, Wang Y. Microstructure and mechanical properties of Ti_2AlNb alloy and C/C composite joints brazed with Ag-Cu-Zn and Ag-Cu-Zn/Cu/Ag-Cu-Ti filler metals. Arch Civ Mech Eng. 2019;19(4):1083-1094. https://doi.org/10.1016/j.acme.2019.04.008.
12. Xing LL, Lin JC, Huang M, Yang WQ. Joining of graphite to copper with Nb Interlayer: microstructure and mechanical properties. Adv Eng Mater. 2019;21(2):1800810. https://doi.org/10.1002/adem.201800810.
13. Duan Y, Mao YW, Xu ZM, Deng QR, Wang GM, Wang SG. Joining of graphite to Ti6Al4V alloy using Cu-based fillers. Adv Eng Mater. 2019;21(11):1900719. https://doi.org/10.1002/adem.201900719.
14. Norouzi E, Shamanian M, Atapour M, Khosravi B. Diffusion brazing of Ti–6Al–4V and AISI 304: an EBSD study and mechanical properties. J. Mater. Sci.2017;52(20):12467-12475. https://doi.org/10.1007/s10853-017-1376-z.
15. Elrefaey A, Tillmann W. Evaluation of transient liquid phase bonding between titanium and steel. Adv. Eng. Mater. 2009;11(7): 556-560. https://doi.org/10.1002/adem.200900021.
16. Vidyuk TM, Dudina DV, Esikov MA, Mali VI, Anisimov AG, Bokhonov BB, Batraev IS. Pulsed current-assisted joining of copper to graphite using Ti-Cu brazing layers. Mater Today: Proc. 2020;25:377-380. https://doi.org/10.1016/j.matpr.2019.12.095.
17. Wei YN, Niu R, Guo HL, Luo YG, Zou JT. Microstructure and performance of graphite/copper joints by brazing with different interfacial structures. Adv Eng Mater. 2022;24(5): 2101161. https://doi.org/10.1002/adem.202101161.
18. Okamoto H, Schlesinger ME, Mueller EM. ASM Handbook Volume 3: Alloy Phase Diagrams. Ohio(OH):

ASM International; 2016.

19. Mao YW, Peng LX, Wang S, Xi LX. Microstructural characterization of graphite/CuCrZr joints brazed with $CuTiH_2Ni$-based fillers. J Alloys Compd. 2017;716:81-87. https://doi.org/10.1016/j.jallcom.2017.05.019.
20. Buenconsejo PJS, Zarnetta R, König D, Savan A, Thienhaus S, Ludwig A. A new prototype two-phase (TiNi)-(β-W) SMA system with tailorable thermal hysteresis. Adv Funct Mater. 2011;21(1):113-118. https://doi.org/10.1002/adfm.201001697.
21. Watanabe M, Adachi M, Fukuyama H. Density measurement of Ti–X (X= Cu, Ni) melts and thermodynamic correlations. J Mater Sci. 2019;54(5):4306-4313. https://doi.org/10.1007/s10853-018-3098-2.
22. Arroyave R, Eagar TW. Metal substrate effects on the thermochemistry of active brazing interfaces. Acta Mater. 2003;51(16):4871-4880. https://doi.org/10.1016/S1359-6454(03)00330-6.
23. Konieczny M. Processing and microstructural characterisation of laminated Ti-intermetallic composites synthesised using Ti and Cu foils. Mater Lett. 2018;62(17-18):2600-2602. https://doi.org/10.1016/j.matlet.2007.12.067.
24. Xiong JT, Peng Y, Zhang H, Li JL, Zhang FS. Microstructure and mechanical properties of Al-Cu joints diffusion-bonded with Ni or Ag interlayer. Vacuum. 2018;147:187-193. https://doi.org/10.1016/j.vacuum.2017.10.033.
25. Hao XH, Dong HG, Li S, Xu XX, Peng L. Lap joining of TC4 titanium alloy to 304 stainless steel with fillet weld by GTAW using copper-based filler wire. J Mater Process Technol. 2018;257:88-100. https://doi.org/10.1016/j.jmatprotec.2018.02.020.
26. Dai J, Yu B, Ruan Q, Ruan QD, Chu PK. Improvement of the laser-welded lap joint of dissimilar Mg alloy and Cu by incorporation of a Zn interlayer. Mater. 2020;13(9):2053. https://doi.org/10.3390/ma13092053.
27. Zhong Z, Hinoki T, Kohyama A. Joining of silicon carbide to ferritic stainless steel using a W-Pd-Ni interlayer for high-temperature applications. Int J Appl Ceram Technol. 2010;7(3):338-347. https://doi.org/10.1111/j.1744-7402.2009.02461.x.
28. Hynes NRJ, Velu PS, Raja MK, Jebaraj DJJ, Benita B. Simulation on graphite to copper joints in nuclear reactor applications by transient liquid phase bonding. Mater. Today: Proc. 2021;47:7095-7098. https://doi.org/10.1016/j.matpr.2021.06.209.
29. Zhong Z, Zhou Z, Ge C. Brazing of doped graphite to Cu using stress relief interlayers. J Mater Process

Technol. 2009;209(5):2662-2670. https://doi.org/10.1016/j.jmatprotec.2008.06.021.

30. Gianchandani PK, Casalegno V, Smeacetto F, Ferraris M. Pressure-less joining of C/SiC and SiC/SiC by a $MoSi_2$/Si composite. Int J Appl Ceram Technol. 2017;14(3):305-312. https://doi.org/10.1111/ijac.12631.
31. Ba J, Ji X, Wang B, Li PX, Lin JH, Qi JL, Cao J. In-situ alloying of BNi2+Ni interlayer for brazing C/C composites and GH3536 Ni-based superalloy. J Manuf Processes. 2021;67:52–55. https://doi.org/10.1016/j.jmapro.2021.04.061.
32. Chen HS, Long CS, Wei TG, Gao W, Xiao HX, Che L. Effect of Ni interlayer on partial transient liquid phase bonding of Zr–Sn–Nb alloy and 304 stainless steel. Mater Des. 2014;60:358–362. https://doi.org/10.1016/j.matdes.2014.03.055.
33. Niu JB, Wang Y, Yang ZW, Wang DP. Microstructure and mechanical properties of titanium–zirconium–molybdenum and Ti_2AlNb joint diffusion bonded with and without a Ni interlayer. Adv Eng Mater. 2019;21(11):1900713. https://doi.org/10.1002/adem.201900713.